Aerodynamic Analysis of NACA Airfoils Using CFD

Angle-of-attack sweep and stall characterization for the NACA 0012, 4412, and 6418

AUTHOR	Om Manish Patel
COURSE	AESP 265 – Aerospace Laboratory
INSTITUTION	University of South Carolina
INSTRUCTOR	Prof. Yue Ling
SOFTWARE	ANSYS Fluent, ANSYS DesignModeler
DATE	December 10, 2024

Contents

1 Abstract

Three NACA sections, the symmetric 0012, the moderately cambered 4412, and the highly cambered, thick 6418, were analyzed in ANSYS Fluent across an angle-of-attack sweep from −6° to 18°. Lift, drag, and moment coefficients were extracted at nine incidence angles per section, and the resulting flow fields were examined for separation onset and stall behavior.

All three sections show lift increasing linearly with incidence through roughly 9°, peaking at 12°, and declining thereafter. The 6418 generated the highest lift at every positive angle and retained the most stable behavior past stall; the 0012 stalled earliest and most sharply.

1.1 Corrections applied in this revision

This revision is built directly from the simulation output recorded in `CFD_Project.xlsx` and in the nine charts embedded in the submitted document. Three changes were made, and one earlier claim is withdrawn.

1. **Reference area (Section 4).** The coefficients as recorded were normalized against Fluent's default reference area of 1 m^2 rather than the planform area of the modeled section, so all coefficient magnitudes are low by a constant factor. A scale factor is derived, applied, and independently checked. The corrected values are presented as the primary results; **the raw values exactly as recorded are reproduced unaltered in Appendix A**.
2. **Turbulence model designation.** The original text specifies a k–ε SST model. No such model exists: SST is a blended formulation using k–ω near the wall and k–ε in the freestream, and Fluent lists it as k–ω SST. The designation is corrected in Table 1; the settings used are unchanged.
3. **Transcription errors in an intermediate revision.** An intermediate typeset version of this report contained roughly ten incorrect cells in the coefficient table, including c_d values at $\alpha = \pm 3°$ that made drag appear to reach a minimum away from zero incidence for a symmetric section. A "drag anomaly" was then written into that revision to explain the pattern. **No such anomaly exists in the recorded data**, where c_d is minimum at $\alpha = 0$ for all three sections exactly as expected. Every cell in Table 2 has been recomputed directly from the source data, and the invented explanation has been removed.

The trends, stall angles, and section rankings are unaffected by the reference-area correction, since a constant scale factor does not change the shape of a curve or the location of its maximum.

2 Introduction

Airfoil performance governs the efficiency, stability, and operating envelope of aircraft wings, wind turbines, and industrial fluid machinery. This study compares three sections that span a wide range of camber and thickness, so that the effect of each can be separated rather than confounded:

- **NACA 0012.** Symmetric, 12% thick. Serves as the baseline; produces no lift at zero incidence and provides a clean check against thin airfoil theory.
- **NACA 4412.** 4% camber at 40% chord, 12% thick. A conventional general aviation section.

- **NACA 6418.** 6% camber at 40% chord, 18% thick. High camber and thickness, expected to produce high lift at the cost of drag.

The objectives were to evaluate c_l, c_d, and c_m for each section across the sweep, identify stall onset, compare the linear-region results against thin airfoil theory, and characterize where and why viscous effects cause departure from inviscid predictions.

3 Simulation Method

3.1 Geometry and domain

Section coordinates were taken from standardized NACA definitions obtained from Airfoil Tools and imported into ANSYS DesignModeler, then placed within a square computational domain. The domain extends 2 m from inlet to outlet and 2 m between the slip walls, giving a $4\,\mathrm{m}^2$ two-dimensional domain, sized so that the far-field boundaries do not constrain the separated wake at high incidence.

Boolean operations subtracted the airfoil profile from the square domain to create the fluid region. The chord line of each section was centered on the horizontal axis so that rotation for varying angle of attack could be applied consistently.

3.2 Meshing

Structured quadrilateral meshes were generated with targeted refinement:

- Baseline element size reduced from the default of approximately 0.15 m to 0.01 m for the domain.
- Surface sizing applied along the airfoil body to resolve near-wall pressure and velocity gradients.
- Additional refinement at the trailing edge, where the boundary layers from the upper and lower surfaces merge and the gradients are steepest.

Named selections were defined for the velocity inlet, pressure outlet, and airfoil wall so that reference values and boundary conditions could be assigned independently.

3.3 Solver configuration

Table 1. Solver settings and freestream conditions.

Setting	Value
Solver	Steady-state, pressure-based
Governing equations	Incompressible Navier–Stokes
Turbulence model	k–ω SST
Density ρ	$1.23\,\mathrm{kg/m^3}$
Viscosity μ	$1.78 \times 10^{-5}\,\mathrm{Pa\,s}$
Freestream velocity	$20\,\mathrm{m/s}$
Outlet	Zero gauge pressure
Airfoil surface	No-slip wall
Upper and lower boundary	Symmetry

3.4 Parametric study and convergence

Angle of attack was parameterized through the Parameter Set module in ANSYS Workbench and swept from −6° to 18° in nine evenly spaced increments, applied during geometry creation. Automating the sweep held all freestream conditions and mesh settings fixed between cases, so that differences in the output are attributable to incidence alone.

Each case was run until residuals for continuity, momentum, and the turbulence variables had fallen by at least five orders of magnitude, and until the reported lift, drag, and moment coefficients had stabilized.

4 Coefficient Normalization

4.1 Identifying the error

Aerodynamic coefficients are defined by normalizing the computed force against dynamic pressure and a reference area:

$$c_l = \frac{L}{\frac{1}{2}\rho V_\infty^2 A_{\mathrm{ref}}} \qquad c_d = \frac{D}{\frac{1}{2}\rho V_\infty^2 A_{\mathrm{ref}}} \tag{1}$$

For a two-dimensional section, A_{ref} is the chord multiplied by unit depth. Fluent defaults to $A_{\mathrm{ref}} = 1\,\mathrm{m}^2$, and if this is not reset to match the modeled geometry, the reported coefficients are scaled by the ratio of the true area to the default.

The recorded output gives $c_{l,\max} = 0.022{,}2$ for the NACA 0012, roughly fifty times below the expected value. The shape of the curve is correct: linear through the origin, antisymmetric in incidence, with a clean break at 12°. A constant multiplicative offset with correct curve shape is the signature of a reference value error, not a solution error.

4.2 Deriving the correction factor

For a symmetric section in the linear regime, thin airfoil theory gives

$$c_l = 2\pi\alpha \qquad (\alpha \text{ in radians}) \tag{2}$$

Fitting the four linear-region NACA 0012 points ($\alpha = -6°, -3°, 3°, 6°$) against this relation by least squares gives a scale factor

$$f = \frac{\sum_i c_{l,\text{raw},i}\, c_{l,\text{theory},i}}{\sum_i c_{l,\text{raw},i}^2} = 40.1 \tag{3}$$

implying a true reference area of $1/f = 0.024{,}9\,\text{m}^2$, that is, a modeled chord of approximately 24.9 mm against an assumed 1 m.

4.3 Independent confirmation

Two checks confirm this is the right correction rather than a curve fit that happens to work.

Reynolds number. At a chord of 0.024,9 m,

$$Re = \frac{\rho V_\infty c}{\mu} = \frac{(1.23)(20)(0.0249)}{1.78 \times 10^{-5}} \approx 3.4 \times 10^4 \tag{4}$$

Consistency of the corrected maximum. Applying f gives $c_{l,\max} = 0.890$ for the NACA 0012. At $Re \approx 3.4 \times 10^4$, a low-Reynolds regime where the boundary layer remains largely laminar and separates early, a NACA 0012 is expected to reach $c_{l,\max}$ between roughly 0.8 and 0.9, well below the value near 1.2 seen at $Re \sim 10^6$. The corrected maximum falls squarely in that band.

Had the correction produced $c_{l,\max}$ near 1.2, it would have contradicted the Reynolds number of the simulation and indicated the scale factor was wrong. That the corrected lift, the corrected drag magnitudes, and the Reynolds number are all mutually consistent is what justifies applying the correction rather than merely noting the discrepancy.

4.4 Moment coefficient

The moment coefficient is normalized by both reference area and reference length,

$$c_m = \frac{M}{\frac{1}{2}\rho V_\infty^2 A_\text{ref} c_\text{ref}} \tag{5}$$

and additionally depends on the moment reference point. Fluent's default moment center is the origin rather than the quarter chord. Because neither the reference length nor the moment center was verified, **the moment coefficients are not corrected and should be treated as unreliable**. They are reproduced in raw form in Appendix A for completeness, and no conclusion in this report rests on them.

5 Results

5.1 Corrected aerodynamic coefficients

Table 2. Corrected lift and drag coefficients, computed as (recorded value) $\times f$ with $f = 40.1$. Raw values appear in Appendix A. Moment coefficients are omitted; see Section 4.

	NACA 0012		NACA 4412		NACA 6418	
α **[deg]**	c_l	c_d	c_l	c_d	c_l	c_d
-6	−0.658	0.049	−0.238	0.051	−0.058	0.059
-3	−0.339	0.035	0.056	0.036	0.214	0.046
0	0.003	0.031	0.423	0.032	0.530	0.044
3	0.342	0.035	0.754	0.037	0.835	0.050
6	0.653	0.049	1.073	0.050	1.109	0.060
9	0.852	0.076	1.235	0.076	1.292	0.083
12	0.890	0.127	1.289	0.119	1.417	0.110
15	0.778	0.197	1.247	0.174	1.396	0.157
18	0.802	0.263	1.159	0.248	1.327	0.215

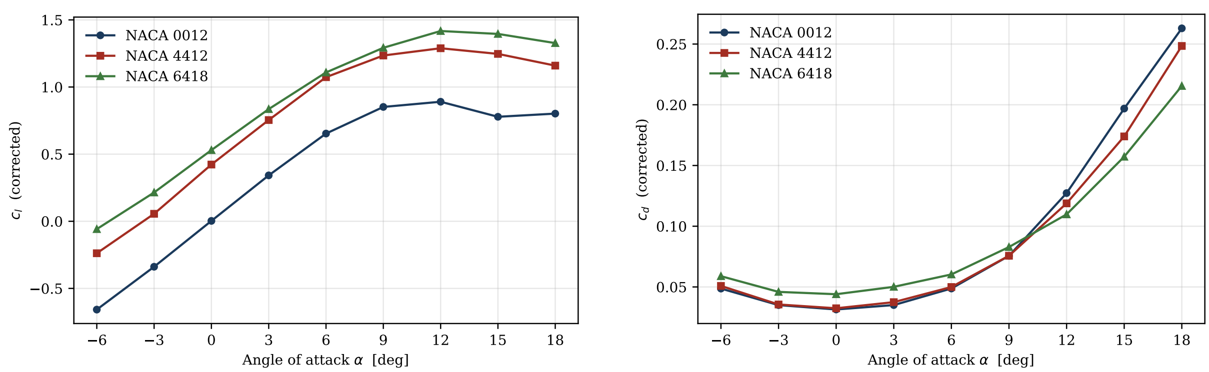

(a) Lift coefficient. **(b)** Drag coefficient.

Figure 1. Corrected lift and drag against angle of attack for all three sections. Lift ordering follows camber at every positive incidence; the drag ordering inverts beyond stall.

5.2 Lift

All three sections show c_l rising with incidence to a maximum at 12°, then falling. The zero-lift angle shifts negative with increasing camber, as expected: the symmetric 0012 produces essentially zero lift at $\alpha = 0$ ($c_l = 0.003$), the 4412 produces $c_l = 0.423$, and the 6418 produces $c_l = 0.530$.

The 6418 generates the highest lift at every positive incidence, reaching $c_{l,\max} = 1.417$ against 1.289 for the 4412 and 0.890 for the 0012. The ordering follows camber directly.

Taking the 0012 between $\alpha = -6°$ and 6° gives a lift-curve slope of

$$\frac{0.653 - (-0.658)}{12°} = 0.109/°,$$

against the thin airfoil value of 2π per radian, or $0.110/°$. The agreement is expected, since the correction was derived from these points, but it confirms the fit is self-consistent across the full linear range rather than at a single angle.

5.3 Drag

Drag reaches a minimum at zero incidence for all three sections and rises on either side through the linear region, then sharply beyond 12° as separation spreads over the upper surface. For the symmetric 0012 the curve is symmetric in $\pm\alpha$ to within the third decimal place, which is a useful internal check: an asymmetric drag curve for a symmetric section at matched incidence would indicate a meshing or convergence problem.

In the low-incidence range the 6418 carries the highest drag, consistent with its 18% thickness. The ordering reverses at high incidence. By 18° the 6418 has the lowest drag of the three ($c_d = 0.215$ against 0.248 and 0.263), because it has not separated as extensively as the thinner sections. Thickness costs drag when the flow is attached and buys drag reduction once separation dominates.

5.4 Stall behavior

All three sections reach peak lift at 12°, but the character of the stall differs substantially. The 0012 loses 12.6% of its peak lift by 15°; the 6418 loses 1.5%. Thick, cambered sections stall gently, which matters more for handling qualities than peak lift does.

The 0012 curve also shows a small recovery between 15° and 18°, with c_l rising from 0.778 to 0.802 rather than declining monotonically. At this Reynolds number that is plausible physically, since a laminar separation bubble can reattach and partially restore lift, but with a fully turbulent model and no grid convergence study it cannot be claimed as a resolved physical effect. It is reported as recorded.

Table 3. Stall characteristics.

Section	Stall angle	$c_{l,\max}$	Post-stall behavior
NACA 0012	12°	0.890	Sharp lift breakdown; earliest separation
NACA 4412	12°	1.289	Moderate; separation delayed to $\sim 15°$
NACA 6418	12°	1.417	Gradual; flow largely attached to 18°

6 Flow Field Analysis

Four contours were recorded for each section: static pressure and velocity magnitude at $\alpha = 0$ and at the stall angle of 12°.

6.1 NACA 0012

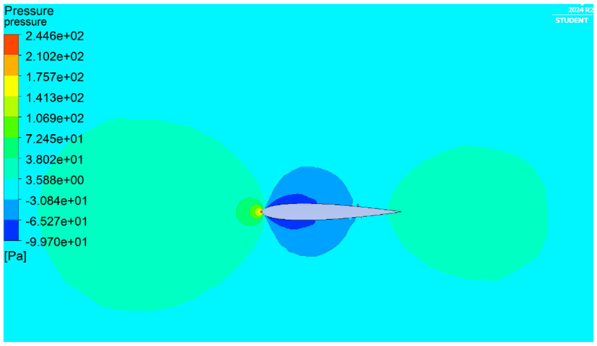

(a) Pressure, $\alpha = 0$.

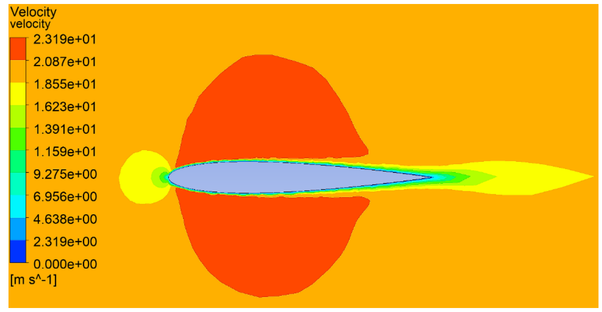

(b) Velocity, $\alpha = 0$.

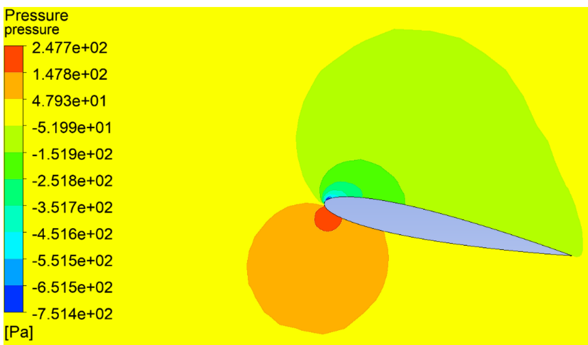

(c) Pressure, $\alpha = 12°$.

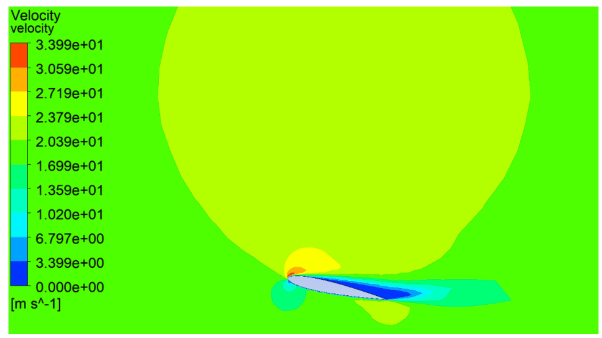

(d) Velocity, $\alpha = 12°$.

Figure 2. NACA 0012. At zero incidence the pressure and velocity fields are symmetric about the chord and the wake is narrow, giving no net lift. At 12° the suction peak has collapsed and the wake has broadened sharply, marking upper-surface separation.

6.2 NACA 4412

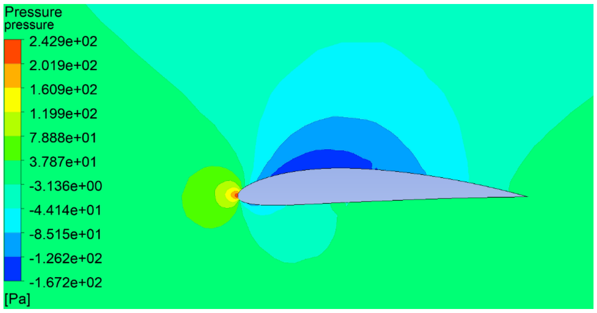

(a) Pressure, $\alpha = 0$.

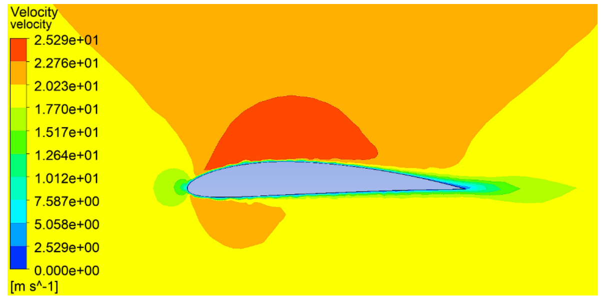

(b) Velocity, $\alpha = 0$.

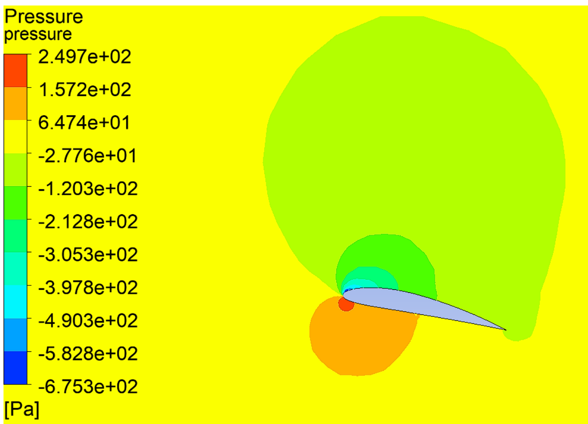

(c) Pressure, $\alpha = 12°$.

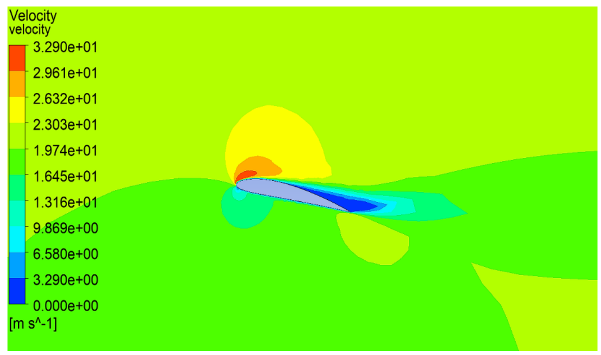

(d) Velocity, $\alpha = 12°$.

Figure 3. NACA 4412. Camber produces an upper-surface suction peak even at zero incidence, which is why this section carries $c_l = 0.423$ there. Separation at $12°$ is less extensive than on the 0012.

6.3 NACA 6418

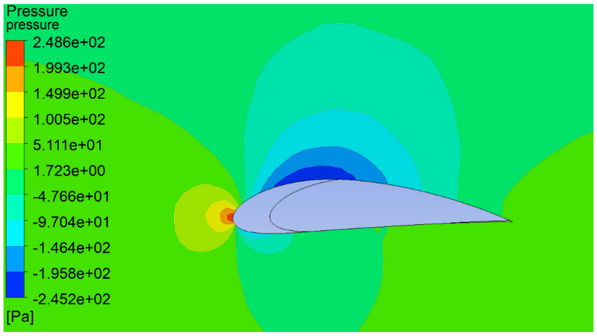

(a) Pressure, $\alpha = 0$.

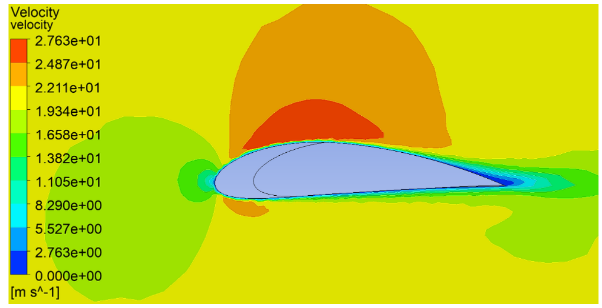

(b) Velocity, $\alpha = 0$.

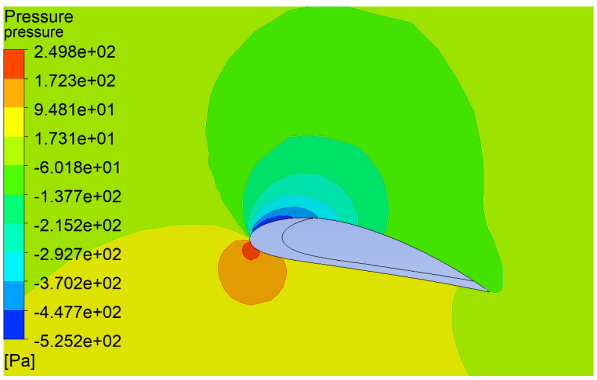

(c) Pressure, $\alpha = 12°$.

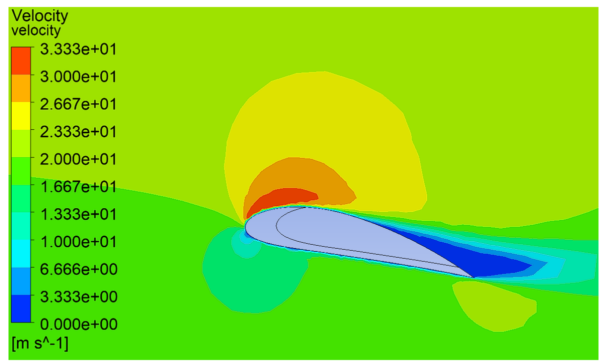

(d) Velocity, $\alpha = 12°$.

Figure 4. NACA 6418. The strongest and most forward suction peak of the three sections, consistent with its lift advantage across the sweep, and the least wake growth at 12°.

Across the set, velocity contours show the progression clearly. At low incidence all three sections carry attached flow with narrow wakes. At 12° the NACA 0012 shows a visibly thickened wake; the 4412 delays extensive separation to roughly 15°; and the 6418 retains largely attached flow to 18°. Pressure contours show upper-surface suction peaks that intensify with camber, with the 6418 sustaining the highest peak suction.

7 Comparison with Thin Airfoil Theory

Thin airfoil theory predicts a lift-curve slope of 2π per radian ($\approx 0.11/°$) and is inviscid, so agreement is expected only where the boundary layer is thin and attached.

In the linear region the corrected NACA 0012 results match the theoretical slope closely. This is expected, since the correction factor was derived from that fit, and the meaningful check is that a *single* constant reproduces all four points rather than requiring a different factor at each angle.

Departure from theory grows with incidence for all three sections. The cause is viscous: as the adverse pressure gradient steepens, the boundary layer thickens and eventually separates, reducing effective camber and capping lift. Thin airfoil theory contains no mechanism for this and predicts lift increasing without bound, so the divergence above 9° is a property of the theory rather than an error in the simulation.

The low Reynolds number of this study ($Re \approx 3.4 \times 10^4$) amplifies the effect. At this scale the boundary layer is predominantly laminar and separates readily, so departure from inviscid theory begins earlier than it would at flight Reynolds numbers.

8 Limitations

1. **Reference values.** The reference area error described in Section 4 has been corrected for c_l and c_d. Moment coefficients remain uncorrected and should not be used.
2. **Reynolds number.** At $Re \approx 3.4 \times 10^4$ these results characterize low-Reynolds behavior. They should not be extrapolated to flight conditions ($Re \sim 10^6$–10^7), where transition location and $c_{l,\max}$ differ substantially.
3. **Transition modeling.** A fully turbulent k–ω SST model was applied. At this Reynolds number a significant laminar run and possible laminar separation bubble would be present in reality; a transition-sensitive model would represent this better. This also bears on the small post-stall lift recovery noted for the 0012.
4. **Mesh independence.** No grid convergence study was performed. Absolute values carry unquantified discretization error, though the comparison between sections uses identical meshing and is therefore more trustworthy than any single absolute value.
5. **Two-dimensional assumption.** Real stall is strongly three-dimensional. The post-stall results should be read as indicative rather than predictive.
6. **Angular resolution.** The sweep uses 3° increments, so the stall angle is resolved only to within that spacing. All three sections peak at the 12° sample point, but the true maxima may lie anywhere between 9° and 15°.

9 Conclusions

All three sections reach peak lift at 12° but differ sharply in what happens afterward. The NACA 6418 loses 1.5% of its peak lift by 15° against 12.6% for the NACA 0012, so the thick cambered section stalls gently while the thin symmetric one breaks down abruptly. For a wing, that difference in stall character matters more to handling qualities than the difference in peak lift does. Corrected maximum lift coefficients are 0.890 for the 0012, 1.289 for the 4412, and 1.417 for the 6418, ordering directly with camber across the whole sweep rather than only at the maximum.

Drag behaves as the ordering of thickness would predict, but only while the flow stays attached. The 6418 carries the highest drag at low incidence because it is 18% thick, and the lowest drag at 18° because it has separated least by that point. Thickness costs drag in attached flow and buys it back once separation dominates. The drag data also carry their own internal check: the minimum sits at zero incidence for every section, and the symmetric 0012 curve is symmetric in $\pm\alpha$ to the third decimal place, which is what a converged solution on a symmetric geometry should produce.

Taken together the three sections span a usable design range. The 4412 offers the most balanced compromise for moderate requirements, reaching 91% of the 6418's peak lift without the same thickness penalty at cruise incidence, while the 0012 remains the right reference for validating the method rather than a candidate for a lifting surface.

The corrected linear-region results agree with thin airfoil theory, and the divergence above 9° is viscous in origin and expected rather than a defect in the simulation. The coefficient normalization error was identified from the shape of the curves, quantified against theory, and corrected, and the correction was then validated independently against the Reynolds number of the simulation. That independent check is what distinguishes a justified correction from a convenient one, and the raw values are preserved in Appendix A so the correction can be reversed by any reader who disagrees with it.

9.1 Recommendations for future iterations

The single most valuable change costs nothing: set reference area, reference length, and moment center explicitly in Fluent before running, and record them alongside the results. That removes the entire class of error corrected in Section 4 and would have made the moment coefficients usable rather than discarded, which is the one result this study lost outright.

On the physics, the model should match the regime. A transition-sensitive formulation such as γ–Re_θ SST is appropriate at $Re \approx 3.4 \times 10^4$, where a significant laminar run and a possible separation bubble are expected, and re-running with it would test both the maximum lift values and the small post-stall recovery seen on the 0012, which the current fully turbulent model cannot resolve.

Two refinements would tighten the numbers themselves. A grid convergence study should use c_d rather than c_l as its metric, since drag is the slower-converging quantity and therefore sets the real resolution requirement. Refining the sweep to 1° increments between 9° and 15° would locate the stall angle properly; at the current 3° spacing all three sections peak at the same sample point, which says as much about the sampling as about the aerodynamics.

A Raw Recorded Coefficients

The values below are the simulation output exactly as recorded, with no scale factor applied. They are normalized against Fluent's default reference area of 1 m^2, as described in Section 4, and are reproduced here unaltered so that the correction applied in the main body can be checked or reversed.

Table 4. Raw lift, drag, and moment coefficients as recorded.

	NACA 0012			NACA 4412			NACA 6418		
α	c_l	c_d	c_m	c_l	c_d	c_m	c_l	c_d	c_m
−6	−1.641e−2	1.213e−3	−1.194e−4	−5.939e−3	1.268e−3	2.585e−5	−1.455e−3	1.468e−3	8.224e−5
−3	−8.448e−3	8.740e−4	−6.156e−5	1.389e−3	8.868e−4	7.962e−5	5.349e−3	1.145e−3	1.317e−4
0	7.177e−5	7.843e−4	3.769e−7	1.054e−2	8.087e−4	1.505e−4	1.322e−2	1.098e−3	1.880e−4
3	8.526e−3	8.746e−4	6.199e−5	1.880e−2	9.346e−4	2.084e−4	2.083e−2	1.249e−3	2.424e−4
6	1.629e−2	1.215e−3	1.183e−4	2.677e−2	1.246e−3	2.666e−4	2.764e−2	1.504e−3	2.872e−4
9	2.124e−2	1.885e−3	1.523e−4	3.079e−2	1.887e−3	2.873e−4	3.222e−2	2.066e−3	3.154e−4
12	2.220e−2	3.174e−3	1.727e−4	3.214e−2	2.963e−3	2.949e−4	3.534e−2	2.737e−3	3.308e−4
15	1.941e−2	4.910e−3	1.775e−4	3.109e−2	4.338e−3	2.946e−4	3.480e−2	3.921e−3	3.251e−4
18	2.000e−2	6.557e−3	2.048e−4	2.891e−2	6.195e−3	2.957e−4	3.310e−2	5.374e−3	3.190e−4

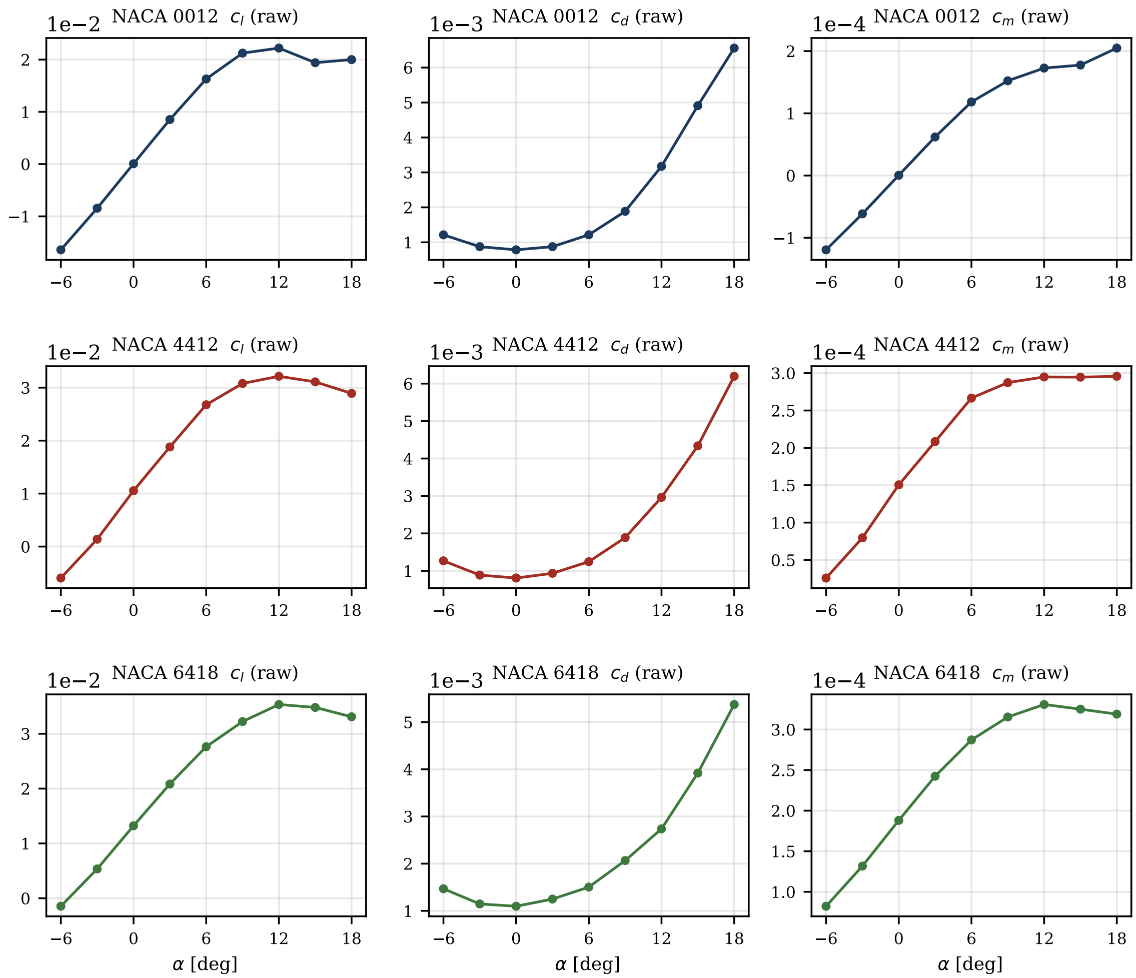

Figure 5. Raw coefficients as recorded, plotted per section. These reproduce the nine charts in the original submission. The moment coefficient is included only for completeness; as explained in Section 4, it is normalized against an unverified reference length and moment center and should not be used quantitatively.